



In situ X-ray absorption study of Cu species in Cu-CHA catalysts for NH₃-SCR during temperature-programmed reduction in NO/NH₃

Chiara Negri, et al. *[full author details at the end of the article]*

Received: 20 October 2020 / Accepted: 30 October 2020 / Published online: 5 January 2021
© The Author(s) 2020

Abstract

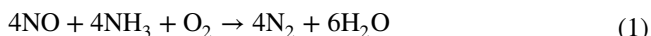
Ammonia-mediated selective catalytic reduction (NH₃-SCR) using Cu-exchanged chabazite zeolites as catalysts is one of the leading technologies for NO_x removal from exhaust gases, with Cu^{II}/Cu^I redox cycles being the basis of the catalytic reaction. The amount of Cu^{II} ions reduced by NO/NH₃ can be quantified by the consumption of NO during temperature-programmed reduction experiments (NO-TPR). In this article, we show the capabilities of in situ X-ray absorption near-edge spectroscopy (XANES), coupled with multivariate curve resolution (MCR) and principal component analysis (PCA) methods, in following Cu^{II}/Cu^I speciation during reduction in NO/NH₃ after oxidation in NO/O₂ at 50 °C on samples with different copper loading and pretreatment conditions. Our XANES results show that during the NO/NH₃ ramp Cu^{II} ions are fully reduced to Cu^I in the 50–290 °C range. The number of species involved in the process, their XANES spectra and their concentration profiles as a function of the temperature were obtained by MCR and PCA. Mixed ligand ammonia solvated complexes [Cu^{II}(NH₃)₃(X)]⁺ (X = OH⁻/O⁻ or NO₃⁻) are present at the beginning of the experiment, and are transformed into mobile [Cu^I(NH₃)₂]⁺ complexes: these complexes lose an NH₃ ligand and become framework-coordinated above 200 °C. In the process, multiple Cu^{II}/Cu^I reduction events are observed: the first one around 130 °C is identified with the reduction of [Cu^{II}(NH₃)₃(OH/O)]⁺ moieties, while the second one occurs around 220–240 °C and is associated with the reduction of the ammonia-solvated Cu-NO₃⁻ species. The nitrate concentration in the catalysts is found to be dependent on the zeolite Cu loading and on the applied pretreatment conditions. Ammonia solvation increases the number of Cu^{II} sites available for the formation of nitrates, as confirmed by infrared spectroscopy.

Keywords Cu-CHA · NH₃-SCR · De-NO_x · X-ray absorption · Multivariate curve resolution · TPR

We dedicate this contribution to Prof. Gianmario Martra, outstanding teacher and scientist.

Introduction

Selective catalytic reduction with NH_3 (NH_3 -SCR) is one of the leading technologies for the abatement of nitrogen oxides (NO_x) from stationary or automotive exhaust gases. In the process, NO is reduced by NH_3 to water and nitrogen, in the presence of oxygen, according to the equation:



Vanadium oxide supported on TiO_2 (VO_x - TiO_2) and Fe- or Cu-exchanged zeolites are currently the best known catalysts for this reaction. VO_x - TiO_2 are usually applied in the treatment of exhaust from large scale stationary plants thanks to low cost, high tolerance to SO_2 , low production of N_2O (a strong greenhouse gas) below 400°C [1]. The more dynamic conditions characterizing diesel vehicles aftertreatment systems require the use of catalyst systems with good activity over a wider temperature range (150 – 500°C) and high hydrothermal stability [2]. These requirements, consistent with the *Euro VI* regulation, are met by the small-pore zeolite Cu-chabazite (Cu-CHA), which is already applied in diesel vehicles thanks to very high NO_x conversion and N_2 selectivity starting from 200°C , coupled with exceptional hydrothermal stability up to 700°C [3–5].

The structure of Cu-CHA is characterized by a very high symmetry. The fact that all T-atom sites of the CHA structure are equivalent, combined with the excellent catalytic properties, makes it an ideal material for modeling studies for NH_3 -SCR [6–11]. The characteristic cage in the CHA structure is surrounded by 6- and 8-member rings, where the exchanged Cu ions, stabilized by the framework Al atoms, are located. The oxidation state of the Cu can be Cu^{I} , which is always anchored to a single Al atom, or Cu^{II} , which can be anchored to either one Al atom (e.g. $[\text{Cu}^{\text{II}}(\text{OH})]^+$) or two Al atoms as a bare Cu^{2+} ion; the latter is often referred to as $\text{Z}_2\text{Cu}^{\text{II}}$, where Z refers to a negative charge on the framework [6]. Many studies have been dedicated to investigate the location, speciation, redox properties and mobility of the Cu ions as a function of temperature and chemical composition (typically expressed as Si/Al and Cu/Al molar ratios or as Cu average volumetric density) in different gas atmospheres [6, 12–16].

In recent years, it has become clear that the SCR reaction involves a reversible transformation between the Cu^{II} and Cu^{I} oxidation states, with the evolution of N_2 and H_2O as products during the reduction step, followed by re-oxidation of Cu^{I} to Cu^{II} [13, 14, 17, 18]. The reaction can be decoupled by following the reduction step in NO/NH_3 and the re-oxidation with NO and O_2 [18, 19]. At low temperatures (200°C), the reduction with NO/NH_3 results in the formation of $[\text{Cu}^{\text{I}}(\text{NH}_3)_2]^+$ complexes [14, 18, 20] which can diffuse between the chabazite cages with affordable energy barriers [7, 13, 21], resulting in some mobility of the $[\text{Cu}^{\text{I}}(\text{NH}_3)_2]^+$ species. These mobile complexes are involved in the re-oxidation step at 200°C in O_2 , forming oxygen-bridged diamino dicopper(II) complexes with general formula $[\text{Cu}_2(\text{NH}_3)_4\text{O}_2]^{2+}$. According to DFT calculations [8], the structure of these dicopper(II) complexes is a side-on μ - η^2 , η^2 -peroxy diamino dicopper(II), which has recently been confirmed by UV-Vis and X-ray spectroscopies [22, 23]. In the reduction half cycle, the mobile $[\text{Cu}^{\text{I}}(\text{NH}_3)_2]^+$ complexes

could also be involved in the oxidative activation of NO [24]. Many aspects of the NH_3 -SCR mechanism, especially in relation to the nature and role of possible reaction intermediates like copper nitrates or nitrites [18, 25–33], NH_4NO_2 and/or NH_4NO_3 , [34], NO^+ [26, 33, 35], HONO and H_2NNO [33] or mixed-ligands Cu complexes such as $[\text{Cu}^{\text{II}}(\text{NH}_3)_3(\text{NO}_3)]^+$ [36] or $\text{Cu}-(\text{N}=\text{O})-\text{NH}_2$ [32], are still under debate. The approaches employed in the literature in order to identify or rule out reaction intermediates are usually based on in situ/*operando* spectroscopies under steady state or transient conditions, pulsed methods such as excitation modulation [32], or transient reaction analysis and chemical trapping techniques [37]. These methods can help in clarifying mechanistic aspects, but they usually only provide qualitative information.

The limited mobility of the $[\text{Cu}^{\text{I}}(\text{NH}_3)_2]^+$ complexes in the Cu-CHA catalysts results in a fraction of the Cu not participating in the NH_3 -SCR reaction [19]. In an attempt to determine the amount of Cu involved in the NH_3 -SCR reaction, temperature-programmed reduction with NO (NO-TPR) was proposed [38]: this technique is meant to measure the amount of NO consumed in heating an oxidized form of Cu-CHA exposed to a NO/ NH_3 mixture, which results in the formation of the $[\text{Cu}^{\text{I}}(\text{NH}_3)_2]^+$ complexes. This approach is based on the idea that the reduction in NO/ NH_3 is actually a part of the NH_3 -SCR cycle, and therefore Cu not participating in the NH_3 -SCR reaction does not contribute to the NO consumption in the reduction either. This method was applied to a series of Cu-CHA catalysts with different Cu/Al and Si/Al ratios, in which the Cu^{II} state preceding the NO-TPR step was obtained by treatment in O_2 at 500 °C or by oxidation of $[\text{Cu}^{\text{I}}(\text{NH}_3)_2]^+$ complexes in NO/O_2 at 50 °C. The latter represents the oxidation half-cycle and implies the formation of copper nitrates $[\text{Cu}^{\text{II}}(\text{NO}_3)]^+$ species [18, 27, 28]. Interestingly, the consumption of NO (reflecting the amount of reducible Cu^{II}) was found to depend not only on the Cu content, but on the ‘history’ of the catalyst as well. Two reduction peaks, assigned to the reduction of Cu-oxide or Cu-hydroxide (Cu-a) and $[\text{Cu}^{\text{II}}(\text{NO}_3)]^+$ (Cu-b), were observed around 130 and 220–240 °C respectively. The activity in the NH_3 -SCR reaction at low temperature (200 °C) was found to correlate linearly with the amount of Cu-b on catalysts pre-reduced in NO/ NH_3 (reduction half-cycle) before the NO/ O_2 oxidation step [38].

In this work, the described NO-TPR procedure [38] has been followed by X-ray absorption spectroscopy (XAS) complemented by infrared, to get molecular level information on the Cu species involved in the process. To this aim, we applied the multivariate curve resolution (MCR) approach to the measured XANES spectra; this technique allows to decompose an experimental dataset into a series of spectra, generated by the species present in the chemical mixture under analysis, each multiplied by its signal-related concentration profile, without any assumption about the individual chemical/physical species that contribute to the global signal response [39].

Experimental

Materials

Two Cu-CHA zeolites with Si/Al=15 and Cu/Al ratios of ca. 0.2 and 0.5 (1.28 and 2.65 wt% Cu, respectively) were obtained by ion-exchange of the parent materials

with a 1.5 mM Cu-acetate solution, followed by calcination at 500 °C for 3 h [38]. These are labeled in the following as 0.2_15 and 0.5_15, respectively, and correspond to the samples B and E (1.23 and 2.63 wt% Cu, respectively) in ref [38].

X-ray absorption spectroscopy (XAS)

In situ XAS data collection.

The in situ XAS data were collected at the BM23 beamline [40] of the European Synchrotron Radiation Facility (ESRF) using the Microtomo reactor cell [41], developed by the ESRF sample environment group. The powdered Cu-CHA catalysts were prepared in the form of self-supporting pellets with masses optimized for transmission-mode XAS measurements (ca. 100 or 120 mg, resulting in $\Delta\mu x = 0.5$ or 0.3 with total absorption after the edge of $\mu x = 2.5$, for Cu-CHA 0.5_15 and 0.2_15, respectively) and placed inside the reactor cell. The temperature of the sample was controlled by the heating system integrated in the Microtomo cell. The total gas flow rate and the composition of the feed were adjusted by a set of mass flow controllers; we have used a total flow rate of 100 ml/min in the XAS measurements.

The in situ Cu K-edge spectra were acquired in transmission mode, employing a double-crystal Si(111) monochromator to scan the incident energy scan, and ionization chambers to detect incident (I_0) and transmitted photons (I_1). A Cu metal foil was measured simultaneously with all the collected XAS spectra by means of a third ionization chamber (I_2), for energy calibration purposes [42, 43]. The chambers were filled with a He/Ar mixture up to 2.2 bar with Ar partial pressure of 0.1 and 0.3 bar for I_0 and $I_{1,2}$ chambers, respectively. The XAS signal as a function of time/temperature during NO-TPR was monitored with acquisitions of ~ 7 min/scan in the 8800–9970 eV energy range. Spectra were collected with constant energy steps of 5 eV in the pre-edge region and 0.3 eV in the XANES region; a uniform sampling step in k -space of 0.08 \AA^{-1} was adopted in the extended region of the spectra. The energy scales in the XANES scans analyzed in this work were aligned using the simultaneously measured data for the Cu metal foil, and normalized to unity edge jump. The Athena software from the Demeter package was used for data analysis [44].

XANES statistical analysis and multivariate curve resolution (MCR).

To assign the measured XANES features to specific Cu-states, we used the multivariate curve resolution (MCR) approach. The data factorization was obtained by the iterative alternating least-squares (ALS) algorithm [45] as follows. Initially, the algorithm requires the determination of the number of pure species in the multicomponent system. This information can either be known beforehand or determined [46] through the application of Principal Component Analysis (PCA) together with some suitable statistical estimators [47]. Afterwards, the MCR-ALS routine must be initialized through the identification of a set of spectra S or concentration profiles C preferentially close to the pure-ones, which can be isolated by the routine. The ALS procedure starts from

this initial estimate, calculating and refining S and C in each iterative cycle until convergence is achieved. Along with this process, different constraints can be applied in order to nudge the result towards a chemically interpretable solution. The algorithm convergence is controlled through a figure of merit called *Lack of Fit* (%LOF), which should not change more than 0.1% between two consecutive iterations at convergence [46].

In the present work, PCA and MCR analyses were carried out by merging the XANES spectra (93 spectra with 124 energy points per spectrum) for all experiments in a global dataset. The MCR-ALS routine was run within a three-PCs model based on PCA outcomes and initialized through the SIMPLISMA method [48]. As constraints, we imposed the non-negativity of the spectral and concentration profiles together with the mass balance condition which, for each scan, foresees the sum to 1 of the concentration values for each chemical species [49]. The refinement converged after 21 iterations with a final %LOF value of 0.57 and a percentage of variance of 99.997%. The output of the algorithm is the MCR-ALS-retrieved XANES spectra S and concentration profiles C .

The quality of the reproduction of the experimental dataset is expressed in terms of % R_{factor} :

$$\% R_{\text{factor}} = \frac{\sum_{i,j} |D - D^{\text{PCA}}|}{\sum_{i,j} |D|}$$

where D and D^{PCA} are the original and the PCA reconstructed dataset, while the subscripts i and j are the respective rows and columns.

DFT-assisted XANES simulations

To assist the interpretation of the Cu K-edge XANES data, the spectra of $[\text{Cu}^{\text{I}}(\text{NH}_3)_2]^+$ and $\text{Z}[\text{Cu}^{\text{I}}(\text{NH}_3)]$ complexes hosted inside the CHA framework were calculated starting from the DFT-optimized structures reported in our previous work [20]. For each geometry, an all-electron single point calculation was performed using PBE exchange–correlation functional [50] implemented in ADF software [51, 52]. A large QZ4P basis set was employed for all atoms in the $\text{Z}[\text{Cu}^{\text{I}}(\text{NH}_3)]$ model and for Cu and its 30 nearest neighbors in the $[\text{Cu}^{\text{I}}(\text{NH}_3)_2]^+$ model (the rest being reproduced by a smaller TZ2P basis), in order to obtain high-quality data for both core and valence orbitals. The resulting molecular orbitals were projected onto a cubic grid centered around the Cu atom. Grid dimensions were 1 Å in each direction with a total of $51^3 = 132,651$ points. The Cu K-edge XANES spectra were obtained by numerical volume integration of the 1 s core orbital with the unoccupied valence orbitals within the dipole approximation, using in-house software previously used for XES [6, 53] and XANES simulations [6, 54, 55].

Infrared spectroscopy

The in situ FTIR spectra were recorded in transmission mode on a PerkinElmer System 2000 infrared spectrophotometer, equipped with a MCT detector averaging 128

interferograms (recorded at 2 cm^{-1} resolution) for each spectrum. The zeolite powders were pressed in the form of self-supporting pellets of ca. 15 mg and placed inside a commercial FTIR reactor cell (AABSPEC, no. 2000-A multimode) with controlled gas atmosphere and temperature. The gas flow used in the experiments was 50 ml/min. The FTIR reactor cell inlet line was heated to $130\text{ }^\circ\text{C}$. The reported spectra are background subtracted, by using a spectrum of the zeolite measured at $50\text{ }^\circ\text{C}$ before NO/O_2 dosage as a reference.

Experimental procedure

To follow the reduction of the Cu in Cu-CHA, in situ XAS and infrared spectra of an oxidized form of the Cu-CHA zeolites were measured during heating from 50 to $290\text{ }^\circ\text{C}$ in NO/NH_3 . In this article we apply two different procedures to prepare the oxidized Cu-CHA, which are depicted in Fig. 1. In the first procedure, the Cu-CHA catalyst is initially exposed to 100% O_2 at $400\text{ }^\circ\text{C}$, cooled down to $50\text{ }^\circ\text{C}$, and then exposed to a mixture of 1000 ppm NO and 10% O_2 . After purging in inert gas (He for XAS, and N_2 for infrared) to remove the O_2 , the catalysts were exposed to a mixture of 1000 ppm NO and 1000 ppm NH_3 at $50\text{ }^\circ\text{C}$, and the system was allowed to equilibrate under these conditions for about 1 h. Then, the temperature was increased to $290\text{ }^\circ\text{C}$ by $1\text{ }^\circ\text{C}/\text{min}$ in the NO/NH_3 mixture, while continuously recording the spectra. This pretreatment procedure is referred to as "OX", because the exposure to the NO/O_2 mixture at $50\text{ }^\circ\text{C}$ is done on an oxidized form of Cu-CHA.

In the second procedure, the exposure to NO/O_2 mixture at $50\text{ }^\circ\text{C}$ is done on a reduced form of Cu-CHA, and is therefore referred to as "RED". To reduce the catalyst, an extra reduction step is introduced in the pretreatment procedure as follows. After heating to $400\text{ }^\circ\text{C}$ in 100% O_2 , the catalyst is cooled down to

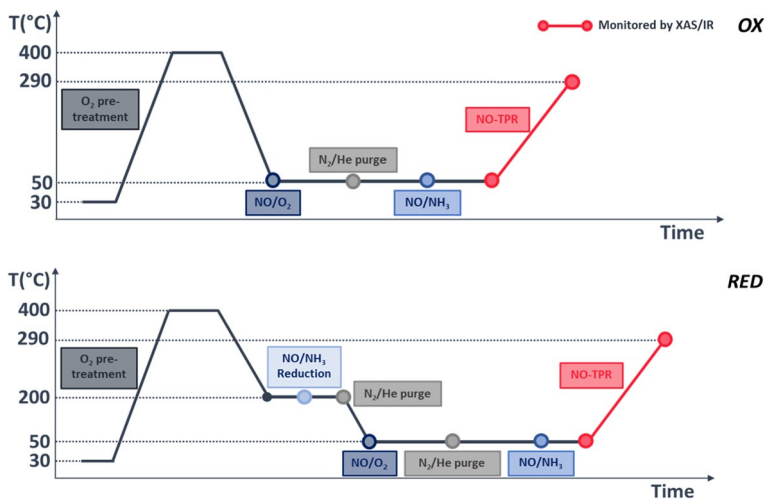


Fig. 1 Schematic representation of the OX (top) and RED (bottom) NO-TPR procedures followed by XAS and infrared. (Color figure online)

200 °C, and exposed to a mixture of 1000 ppm NO and 1000 ppm NH₃ for about 1 h, which reduces the Cu-CHA catalyst. Then, the cell is purged with inert gas, cooled down to 50 °C, and exposed to a mixture of 1000 ppm NO and 10% O₂. From here, the procedure is identical to the "OX" procedure, described above.

Results and discussion

NO-TPR experiments

Figure 2 summarizes typical NO consumption profiles observed during heating in NO/NH₃ for two Cu-CHA catalysts with Si/Al = 15 and a Cu content of 1.23 wt% and 2.63 wt% respectively, as published earlier in ref [38], showing the different reduction behavior after the OX and RED treatments. In NO-TPR, two NO consumption peaks can be observed at around 130 °C and 220–240 °C. The peak at 220–240 °C is only observed after pretreatment of the catalyst with NO/O₂, and is thus assigned to a Cu^{II} nitrate-like species [38]; the peak at 130 °C also occurs only after exposure to O₂, and is therefore assigned to a Cu-oxide or hydroxide species. [38]. The Cu-nitrate peak for oxidized Cu-CHA is weak at lower Cu content (0.2_15 OX) and it becomes more prominent at higher Cu content (0.5_15 OX). For a reduced Cu-CHA catalyst (RED), the peak at 220–240 °C is significantly enhanced.

The two reduction events can be related to the following reactions for either Cu oxide or Cu hydroxide:

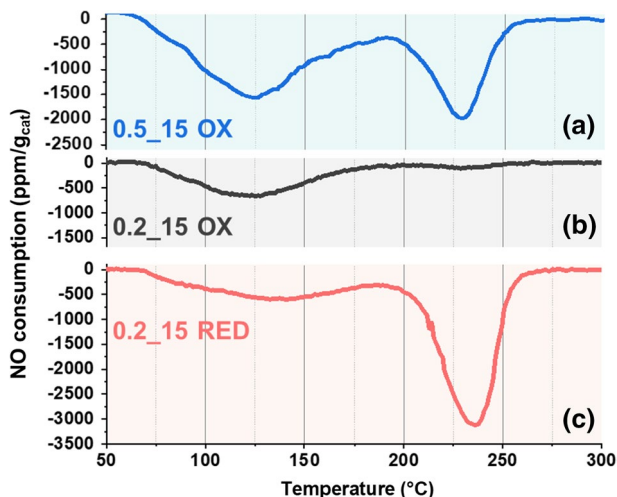
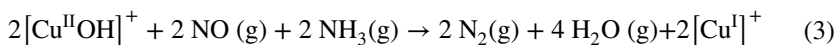
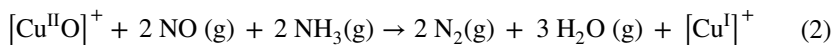
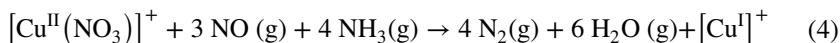


Fig. 2 NO-TPR profiles for the investigated Cu-CHA catalysts pre-exposed to the NO/O₂ mixture at 50 °C. The NO consumption was measured during a ramp in NO/NH₃, after equilibration at 50 °C. The NO/O₂ exposure was preceded by treatment in O₂ at 500 °C in **a** and **b**, and by a reduction in NO/NH₃ at 200 °C in **(c)**. Adapted from ref. [38]



and for Cu-nitrate:



This implies that the stoichiometric NO/Cu ratio for the reduction peak at 130 °C is expected to be between 1 and 2, depending on the nature of the Cu^{II}-oxide/hydroxide species, while this ratio is 3 for Cu-nitrate, with a peak at 220–240 °C [38]. These stoichiometric ratios were employed to quantify the amount of reduced Cu^{II} in the different conditions from the integrated peak areas reproduced in Fig. 1, which was found to be proportional to the NH₃-SCR activity [38].

XANES spectral evolution during NO-TPR

XAS represents an ideal technique to probe, in an element selective fashion, the electronic and structural modifications involving Cu ions hosted inside the zeolitic framework [5, 43, 56] during conditions equivalent to those employed in laboratory NO-TPR experiments discussed above [38]. The X-ray absorption near-edge structure (XANES) region at Cu K-edge contains plenty of spectral fingerprints, enabling an accurate determination of oxidation state and coordination geometry of Cu-species [57–59]. The sensitivity of XANES is sufficiently high for a fast data collection, which allows to follow the dynamic changes in Cu-speciation inside the zeolite framework [15, 60].

Figure 3 reports the in situ Cu K-edge XANES data for the 0.5_15 and 0.2_15 Cu-CHA catalysts following the OX and RED procedures during the reduction of Cu in the NO/NH₃ mixture in the range 50–290 °C, which corresponds to the NO-TPR analysis [38]. The overall observations in the three experiments are quite similar. At the start of each measurement, when the Cu^{II} state has been exposed to the NO/NH₃ mixture at 50 °C, the XANES spectrum is similar to that of the [Cu^{II}(NH₃)₄]²⁺ model compound in solution, indicating that reduction to Cu^I has not taken place yet. However, there are some characteristic spectral differences with the XANES spectrum of [Cu^{II}(NH₃)₄]²⁺, including smoother features at 8994 and 8999 eV in the white-line peak region and a weaker and broader rising-edge peak at ca. 8986 eV, stemming from 1 s → 4p transition in Cu^{II} ions. Consistently with previous works, these differences indicate that the Cu^{II} species formed under these conditions retain a pseudo-square planar coordination geometry, but with Cu^{II} centers bonded to three NH₃ molecules and an O-containing ligand [13, 36, 60]. This could be related to a combination of mixed-ligand mobile [Cu^{II}(NH₃)₃(NO₃)]⁺ complexes [36] and other fourfold coordinated NH₃-solvated Cu^{II} species, such as [Cu^{II}(NH₃)₃(OH)]⁺ [60].

Heating in NO/NH₃ leads to a progressive development of the characteristic XANES features for a linear Cu^I species. In particular, a prominent rising-edge peak at ca. 8983 eV develops [18, 57, 61], accompanied by the decrease in the white-line

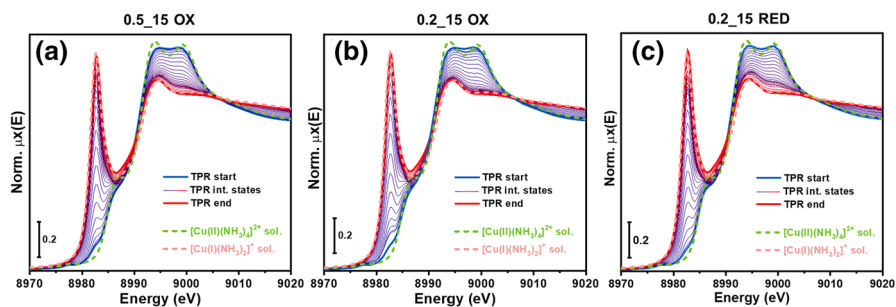


Fig. 3 In situ Cu K-edge XANES spectra obtained during NO-TPR in a NO/NH₃ flow from 50 (blue lines) to 290 °C (red lines) for: **a** Cu-CHA 0.5_15 OX; **b** Cu-CHA 0.2_15 OX; **c** Cu-CHA 0.2_15 RED. XANES spectra of the [Cu^{II}(NH₃)₄]²⁺ and [Cu^I(NH₃)₂]⁺ model compounds, measured in solution phase, are reported for comparison as green and pink dashed lines, respectively. (Color figure online)

peak intensity. Furthermore, the weak pre-edge peak at ca. 8977 eV, related to $1s \rightarrow 3d$ dipole-forbidden transitions in Cu^{II} ions, disappears. These spectral fingerprints are also reflected in the XANES of the [Cu^I(NH₃)₂]⁺ model compound, which is included in Fig. 3 for comparison. In agreement with previous reports, some differences are observed with respect to the spectrum of [Cu^I(NH₃)₂]⁺ at increasing temperature (from 200 °C upward), particularly in the shape of the white-line peak. This has been attributed to the formation of Z[Cu^I(NH₃)] species, where a Cu^I center is coordinated to an oxygen atom of the zeolite framework and to an ammonia ligand molecule, in a quasi-linear fashion [22, 60]. This means that the [Cu^I(NH₃)₂]⁺ complexes formed by reduction in NO/NH₃ release an NH₃ ligand above 200 °C and subsequently lose their mobility [13, 14, 62].

In the following, we apply statistical analysis and multivariate curve resolution (MCR) to the whole XANES dataset reported in Fig. 3, in order to obtain quantitative information on the evolution of Cu-speciation as a function of the temperature in the three NO-TPR experiments.

Principal component analysis (PCA) and multivariate curve resolution (MCR) of in situ XANES

The estimation of the number of spectroscopically distinguishable chemical species causing the XANES spectral variations observed in Fig. 3 and the subsequent isolation of their related spectral contributions has been realized by considering the entire XANES data set in the three measurements. The principal components (PCs) present in the XANES dataset are then identified by applying PCA on this data set. This approach allows to lower the ambiguity in the reconstruction typical of the MCR-ALS algorithm, which results in an improved identification of the PCs and the corresponding concentration profiles [15].

First, the variance related to each principal component (PC) is plotted in the so-called scree plot (Fig. 4a) [39]. PCs related to chemically or physically interpretable phenomena are characterized by high variances, while a low and approximately stable variance points to noise effects. The elbow of the scree plot curve,

which divides the signal-related PCs from the noise-related ones thus allows to identify the number of chemically significant species in the studied process. For the data in Fig. 4a, the elbow is localized around the third and fourth PC, pointing to the existence of four chemical species. However, a detailed analysis of PCs intensity vs energy (Fig. 4b) shows that the fourth component (PC4) only shows very weak features if compared to PC3, suggesting that PC4 is a minor species. Neglecting PC4 in the description of the global XANES series the $\%R_{\text{factor}}$ value is 0.4%, indicating an optimal reproducibility of the dataset with three PCs only.

Figure 5 reports an overview of the MCR-ALS results, in terms of pure XANES spectra for the three PCs (Fig. 5a) and their respective concentration profiles during heating in NO/NH₃ (Fig. 5c). In agreement with the qualitative considerations provided above, MCR reveals that a Cu^{II} component (PC1, blue curve and bars in Fig. 5) dominates at low temperature in all three experiments. The corresponding MCR-retrieved spectrum exhibits all the features previously discussed as characteristic of fourfold coordinated, mobile Cu^{II} complexes with mixed ligation to N and O atoms in the first coordination sphere [13, 36, 60], as illustrated in Fig. 5c, blue box. The quality of the reconstruction is sufficient to identify the weak pre-edge peak at ca. 8977 eV, which is an unambiguous diagnostic for a Cu^{II} species. This spectral feature is absent in the Principal Component spectra for PC2 and PC3, which therefore both correspond to a Cu^I species.

In line with the smooth decrease in the scree plot between the third and fourth component (Fig. 5a), we believe that PC1 should be connected with a pool of structurally similar mobile Cu^{II} amino-complexes, globally accountable as [Cu^{II}(NH₃)₃(X)]⁺, where X=OH⁻, O⁻ or NO₃⁻. The simultaneous presence of multiple Cu^{II} species, spectroscopically indistinguishable within the energy-resolution of the available (conventional) XANES dataset and inherently merged in

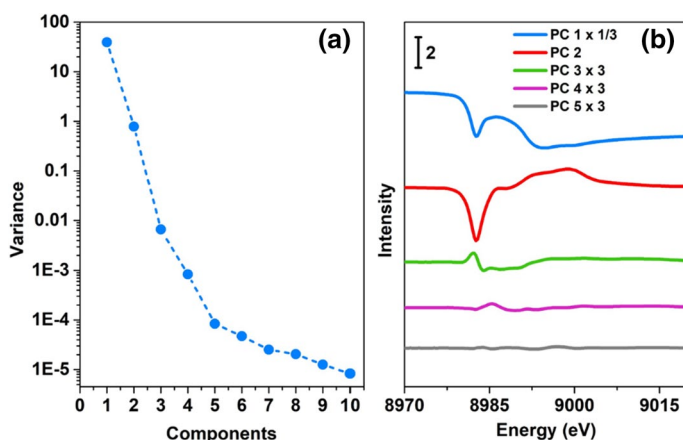


Fig. 4 **a** Scree plot: Data set variances associated to each principal component (PC) plotted vs the components number. **b** Plot of the intensity of each dataset component extracted through the PCA vs energy. The PC intensity was arbitrarily multiplied for the indicated factor for easier comparison

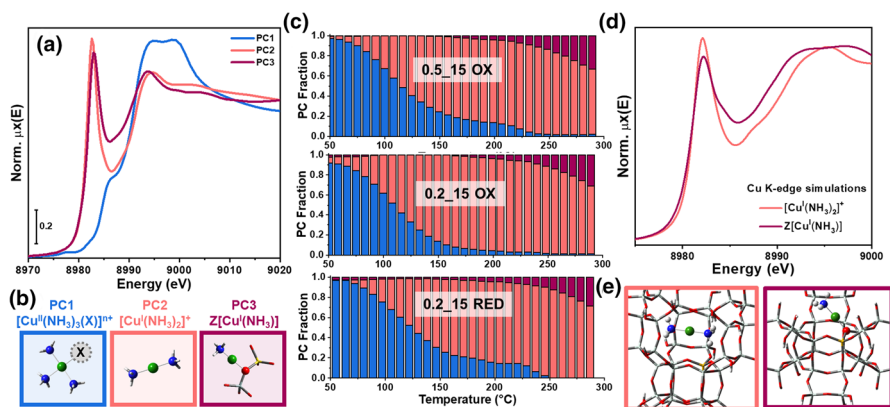


Fig. 5 Results of MCR analysis applied to the global in situ XANES dataset reported in Fig. 2. **a** MCR-retrieved Cu K-edge XANES spectra of the three PCs evidenced by PCA. **b** Pictorial illustration of the pure Cu-species assigned to the MCR-retrieved spectra in part **a**, using the same color code. **c** Concentration profiles for each PC (same color code) as a function of the temperature during NO-TPR on Cu-CHA 0.15_15 OX, Cu-CHA 0.12_15 OX and Cu-CHA 0.15_15. **d** DFT-assisted Cu K-edge XANES simulations, computed from the DFT-optimized structures **e** of mobile $[\text{Cu}^{\text{I}}(\text{NH}_3)_2]^+$ complexes and framework-coordinated $\text{Z}[\text{Cu}^{\text{I}}(\text{NH}_3)]$. (Color figure online)

the PC1 contribution, is in agreement with the observation of multiple reduction events in NO-TPR (Fig. 2).

The MCR results in Fig. 5 show that PC1 is gradually converted a linear Cu^{I} species (PC2, pink curve and bars in Fig. 5) when heated in the NO/ NH_3 mixture. The corresponding MCR-retrieved XANES spectrum is in excellent agreement with that of solution-phase $[\text{Cu}^{\text{I}}(\text{NH}_3)_2]^+$ (Fig. 4, pink dashed line), supporting the assignment of PC2 to this Cu^{I} complex, illustrated in Fig. 5c, pink box. This $[\text{Cu}^{\text{I}}(\text{NH}_3)_2]^+$ complex is the well-known mobile Cu^{I} species, playing a crucial role in the NH_3 -SCR reaction [7, 19].

Interestingly, MCR analysis also reveals a second quasi-linear Cu^{I} species (PC3, purple curve and bars in Fig. 5). This species starts to form at about 150–200 °C in all three experiments, and progressively increases in concentration at the expense of the $[\text{Cu}^{\text{I}}(\text{NH}_3)_2]^+$ complex at higher temperatures, finally accounting for 28–33% of the total amount of Cu at 290 °C. The MCR-retrieved spectra of PC2 and PC3 show an overall similarity, indicating a similar coordination geometry of the Cu^{I} centers: this difference could not be discerned by a simple linear combination fit analysis. The spectrum of PC3 shows an enhanced normalized absorption at ca. 8987 eV, around the minimum between the rising edge and white-line peaks, and the characteristic rising edge peak, corresponding to a $1s \rightarrow 4p$ transition, is less intense. Furthermore, there are differences in the energy position and shape of the white-line peak. The PC3 resembles a $\text{Z}[\text{Cu}^{\text{I}}(\text{NH}_3)]$ species observed in the Cu K-edge XANES in Cu-CHA in a NH_3 -TPD procedure [60] and also in the reaction of NO with the mobile $[\text{Cu}_2(\text{NH}_3)_4\text{O}_2]^{2+}$ complexes [22]. Therefore, PC3 is assigned to a framework-coordinated quasi-linear Cu^{I} species formed by thermal desorption of one ammonia ligand molecule from the

mobile $[\text{Cu}^{\text{I}}(\text{NH}_3)_2]^+$ complex, which we denote as $\text{Z}[\text{Cu}^{\text{I}}(\text{NH}_3)]$ (Fig. 5c, purple box).

To support the assignment of PC3 to a $\text{Z}[\text{Cu}^{\text{I}}(\text{NH}_3)]$ species, we computed the theoretical Cu K-edge XANES spectra of both the mobile $[\text{Cu}^{\text{I}}(\text{NH}_3)_2]^+$ complex and framework-coordinated $\text{Z}[\text{Cu}^{\text{I}}(\text{NH}_3)]$ species hosted inside the CHA zeolite lattice, after optimization of their geometry by DFT. Figure 5d and e shows these computed XANES spectra, and the structure models employed in the calculations, respectively. The differences in the two computed curves are fully consistent with those observed in the MCR-retrieved spectra for PC2 and PC3, shown in Fig. 5a using the same color code. The $\text{Z}[\text{Cu}^{\text{I}}(\text{NH}_3)]$ features a less intense rising-edge peak, a higher intensity around the minimum between rising edge and white line, as well as a slight shift of the white-line resonance to lower energy with respect to what is predicted for mobile $[\text{Cu}^{\text{I}}(\text{NH}_3)_2]^+$. These results conclusively prove that mobile $[\text{Cu}^{\text{I}}(\text{NH}_3)_2]^+$ is stable in the CHA zeolite only within a limited temperature window. Upon heating above 200 °C, Cu^{I} ions start to lose a single NH_3 ligand, resulting in Cu^{I} ions fixed to the zeolite lattice via a lattice O atom.

Comparison to NO-TPR

Starting from the MCR-concentration profiles reported in Fig. 5c, we can examine the temperature-dependent evolution of Cu^{II} (PC1) and Cu^{I} (PC2+PC3) during the three experiments monitored by XANES (Fig. 6, top panels). In all cases, reduction to Cu^{I} is completed in the 240–250 °C range. However, depending on the sample composition and pretreatment conditions, multiple inflection points can be observed, which can be linked to the reduction events observed in the NO-TPR experiment (Fig. 2), involving the different Cu^{II} species collectively contributing to the PC1 component. To facilitate their visual identification, we have plotted the first-derivative curves of the temperature-dependent $\text{Cu}^{\text{II}}/\text{Cu}^{\text{I}}$ concentration profiles (Fig. 6, middle panels), exhibiting well-defined maxima corresponding to the inflection points. To make the comparison with the NO-TPR experiments easier, the corresponding NO consumption profiles from Fig. 2 are also reported (bottom panels). In this qualitative comparison, one has to remember that the NO consumption peak at 220–240 °C corresponds to a NO/Cu stoichiometry equal to 3, meaning that 3 NO molecules are consumed while only one Cu^{II} ion is reduced, according Eq. (4) [38], which, of course, affects the observed intensities in the XANES and NO-TPR data accordingly.

For Cu-CHA 0.5_15 OX (Fig. 6a), we observe two inflection points at ca. 108 °C and 223 °C. Most of the Cu undergoes reduction in correspondence with the low-temperature reduction event, reaching a Cu^{I} percentage of 87% at 200 °C. The second inflection point, albeit clearly detectable, only involves the reduction of a minor fraction (13%) of Cu, leading to the complete reduction of the Cu in the catalyst. These two reduction phenomena reproduce quite nicely the NO consumption peaks detected in parallel laboratory NO-TPR experiments (bottom panel). Similarly, Cu-CHA 0.2_15 OX (Fig. 6b) exhibits one main low-temperature reduction event, which yields up to 95% Cu^{I} species. In very good agreement with the measured

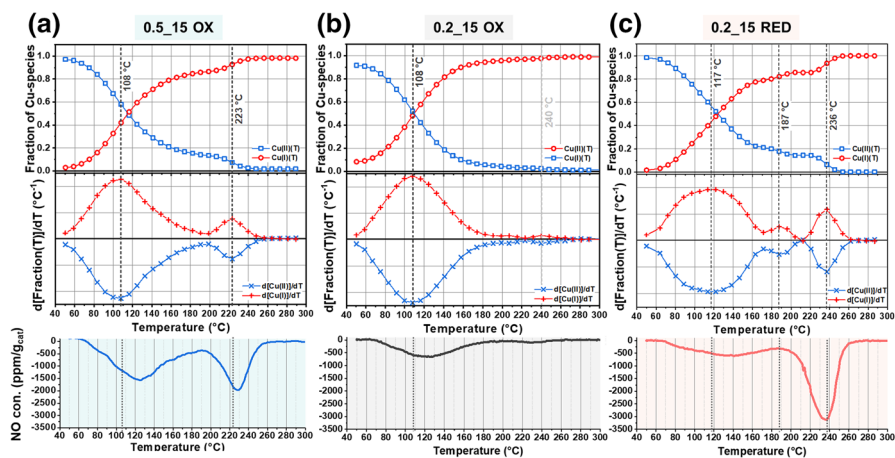


Fig. 6 Comparative overview of temperature-dependent concentration profiles (top panels) for Cu^{II} (blue symbols, given by the concentration of PC1) and Cu^{I} (red symbols, given by the sum of concentrations for PC2 and PC3) and their first derivatives (middle panels) for: **a** Cu-CHA 0.15_15 OX; **b** Cu-CHA 0.12_15 OX; **c** Cu-CHA 0.15_15 RED. Vertical dashed lines highlight temperature values corresponding to the maxima in the first derivatives (inflection points in the concentration profiles) observed from XANES analysis in the three experiments. Bottom panels report for direct comparison the NO consumption profiles from Fig. 2 [38]. (Color figure online)

NO consumption (bottom panel), the high-temperature reduction event is barely observable.

The NO-TPR profile measured by XANES on Cu-CHA 0.2_15 RED (Fig. 6c) is more complex, showing a broad reduction event in the 70–190 °C range (involving the reduction of 80% of Cu^{II} , see top panel) followed by two distinct events at higher temperature. Both the broadness of the low-temperature event and the position of the NO-TPR around 240 °C match the NO consumption peaks well (bottom panel). However, the reduction event around 190 °C, as detected by XANES, is not resolved in the NO-TPR. The quantity of Cu^{II} reduced at high temperature is around 49% according to the NO consumption [38].

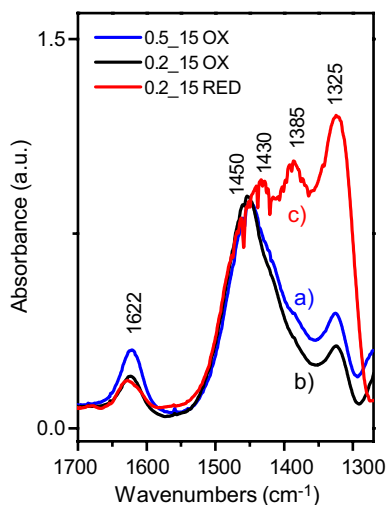
The interpretation of the NO consumption is that the peak at 130 °C is related to a Cu^{II} -oxide or hydroxide, while the one at 220–240 °C is related to a Cu nitrate-like species, according to Eqs. (2)–(4). From our XANES analysis, it follows that all Cu^{II} moieties are solvated by NH_3 as $[\text{Cu}^{\text{II}}(\text{NH}_3)_3(\text{X})]^+$ complexes, where X stands for OH^- , O^- or NO_3^- , and therefore mobile. All these complexes have a pseudo-square planar geometry, resulting in very similar Cu K-edge signatures in XANES. Although a direct spectral discrimination among the Cu^{II} species is not feasible within the energy resolution of the available dataset, they can be effectively resolved through the detection of multiple reduction events, once the Cu^{I} speciation is properly determined by MCR analysis.

As a final consideration, we can put forward some molecular interpretation about the differences in NO consumption during NO-TPR on samples with different pretreatments (compare 0.2_15 OX and 0.2_15 RED in Figs. 2 and 6) and different Cu loading (compare 0.5_15 OX and 0.2_15 OX in the same Figures). The

amount of Cu^{II} that is reduced around 220–240 °C increases with Cu loading and when the sample is pretreated in NO/NH_3 before the NO/O_2 step (RED procedure, see Fig. 1). According to our results, this Cu^{II} species can be described as a mixed-ligand $[\text{Cu}^{\text{II}}(\text{NH}_3)_3(\text{NO}_3)]^+$ complex, with a nitrate group linked in a monodentate fashion, as demonstrated by Negri et al. [36]. In a previous publication, we have also shown that $[\text{Cu}^{\text{II}}(\text{NO}_3)]^+$ are preferentially formed from framework coordinated $[\text{Cu}^{\text{II}}(\text{OH})]^+$ sites, while Cu^{II} ions stabilized by two negative charges on the framework (often referred to as $\text{Z}_2\text{Cu}^{\text{II}}$) are not able to form nitrates, probably due to their strong interaction with the framework [28]. This then leads to the hypothesis that the pretreatment in NO/NH_3 increases the number of Cu^{II} sites available for the formation of nitrates, by solvating and mobilizing both $[\text{Cu}^{\text{II}}(\text{OH})]^+$ and $\text{Z}_2\text{Cu}^{\text{II}}$ ions. This interpretation can also explain the differences observed in samples with different Cu loading, following the hypothesis that $[\text{Cu}^{\text{II}}(\text{OH})]^+$ sites start to be filled after saturation of $\text{Z}_2\text{Cu}^{\text{II}}$ [13].

To support this hypothesis, we compare the infrared spectra for all three cases after equilibration of the NO/NH_3 mixture at 50 °C corresponding to the point where the heating starts. The spectra obtained on the two catalysts after the OX pretreatment (curves a and b in Fig. 7) are similar to those observed by Negri et al. at 50 °C after a similar treatment, which were assigned to a mobile mixed-ligand $[\text{Cu}^{\text{II}}(\text{NH}_3)_3(\text{NO}_3)]^+$ compound [36]. More precisely, the band at 1622 cm^{-1} is assigned to the bending mode of the ammonia molecules bound to the Cu ions (δ_{NH_3}), and the peak at 1325 cm^{-1} corresponds to a symmetric stretching mode of the covalently linked monodentate nitrates ($\nu_{\text{NO}_2\text{sym}}$). The corresponding antisymmetric mode ($\nu_{\text{NO}_2\text{asym}}$, 1430 cm^{-1}) falls in the broad and intense absorption centered at 1440 cm^{-1} , related to ammonium ions ($\delta_{\text{NH}_4^+}$), formed by interaction of ammonia with the Brønsted H^+ sites in the zeolite [20]. The intensity of the NH_3 band (1622 cm^{-1}) is almost doubled in 0.5_15 OX with respect to 0.2_15 OX, in agreement with the higher Cu content. This vibration is not very sensitive to the

Fig. 7 Infrared spectra measured at the beginning of the NO-TPR ramp, after equilibration of the samples in NO/NH_3 at 50 °C for: **a** Cu-CHA 0.15_15 OX; **b** Cu-CHA 0.12_15 OX; **c** Cu-CHA 0.15_15 RED. Spectra are background subtracted and normalized with respect to pellet thickness



local environment (NH_3 being a strong base) so that it likely includes the signals related to all ammonia-solvated Cu^{II} ions (that is $[\text{Cu}^{\text{II}}(\text{NH}_3)_3(\text{X})]^+$, where $\text{X}=\text{OH}^-/\text{O}^-$ or NO_3^-). Interestingly, the intensity of the peak at 1325 cm^{-1} related to the nitrates ligand is higher on sample 0.5_15 OX, in agreement with the NO-TPR results discussed above.

The intensity of the band at 1325 cm^{-1} is much higher when NO/ NH_3 is dosed on NO/ O_2 after pretreatment in NO/ NH_3 (RED procedure, see Fig. 1 and curve c in Fig. 7). This result is in very good agreement with the assignment of the high-temperature peak measured by NO consumption during NO-TPR to Cu nitrate species (Eq. 4 and Ref. [38]), which has been characterized in this work as a mobile $[\text{Cu}^{\text{II}}(\text{NH}_3)_3(\text{NO}_3)]^+$ compound. While XANES is not able to discriminate between $[\text{Cu}^{\text{II}}(\text{NH}_3)_3(\text{OH})]^+ / [\text{Cu}^{\text{II}}(\text{NH}_3)_3(\text{O})]^+$ and $[\text{Cu}^{\text{II}}(\text{NH}_3)_3(\text{NO}_3)]^+$ complexes, infrared clearly shows important differences in the ligands surrounding the Cu^{II} ions. We also acknowledge the formation of ammonium nitrate (band at 1385 cm^{-1} , also present in minor amount in sample 0.5_15 OX), which is known to decompose below $200\text{ }^\circ\text{C}$ nonetheless [34], and is not likely to be involved in the NO consumption peak at higher temperature and in the reduction of Cu^{II} monitored by XAS. Therefore, the results shown in Fig. 7 strongly support the hypothesis that the interaction with NO/ O_2 to form copper nitrates only involves a fraction of the present Cu ions, unless these are mobilized by the interaction with ammonia molecules, which makes them more accessible and thus reactive.

Conclusions

NO-TPR has been recently proposed as a method to quantify the amount of Cu^{II} ions reduced by a NO/ NH_3 mixture in Cu-CHA catalyst active in the NH_3 -SCR reaction. This method involves the pretreatment of the catalysts in different atmospheres (oxidizing or reducing), followed by oxidation (NO/ O_2) and reduction (NO/ NH_3) SCR half cycles at low temperature ($50\text{ }^\circ\text{C}$). NO consumption is then measured during a temperature ramp in NO/ NH_3 to quantify the amount of reducible Cu^{II} ions.

In this work, the speciation of $\text{Cu}^{\text{II}}/\text{Cu}^{\text{I}}$ ions during the NO-TPR experiment has been followed by XANES on two Cu-CHA catalyst with Si/Al ratio of 15 and Cu/Al $\cong 0.2$ and 0.5. The effect of the different pretreatment conditions was also followed on one of the samples in order to investigate the Cu species involved in the low ($130\text{ }^\circ\text{C}$) and high ($220\text{--}240\text{ }^\circ\text{C}$) NO consumption events, assigned to Cu^{II} oxo/hydroxo and nitrate species respectively [38].

Multivariate curve resolution (MCR) and principal component analysis (PCA) methods were applied to the whole dataset of XANES measured in the three experiments, to determine the number of species involved in the process, as well as their respective XANES spectra and concentration profiles as a function of temperature. The results point to the presence of mixed ligand ammonia solvated complexes at the beginning of the experiment, described as $[\text{Cu}^{\text{II}}(\text{NH}_3)_3(\text{X})]^+$, where $\text{X}=\text{OH}^-/\text{O}^-$ or NO_3^- . These are transformed into mobile $[\text{Cu}^{\text{I}}(\text{NH}_3)_2]^+$ complexes, which gradually lose an ammonia ligand and become framework-coordinated $\text{Z}[\text{Cu}^{\text{I}}(\text{NH}_3)]$ approximately above $200\text{ }^\circ\text{C}$.

Although direct spectral discrimination among $[\text{Cu}^{\text{II}}(\text{NH}_3)_3(\text{OH})]^+$ / $[\text{Cu}^{\text{II}}(\text{NH}_3)_3(\text{O})]^+$ and $[\text{Cu}^{\text{II}}(\text{NH}_3)_3(\text{NO}_3)]^+$ species is not feasible within the energy resolution of the available dataset, they can be effectively resolved through the detection of multiple reduction events, once the Cu^{I} speciation is properly determined by MCR analysis. We can thus conclude that the Cu^{II} oxo/hydroxo and nitrates species reduced during the NO-TPR experiment are present as ammonia solvated mobile ions. Moreover, infrared spectroscopy supports the hypothesis that the increase in $[\text{Cu}^{\text{II}}(\text{NH}_3)_3(\text{NO}_3)]^+$ species after a pretreatment with NO/ NH_3 is due to the solvating effect of ammonia, which increases the number of Cu^{II} available for the reaction with NO/ O_2 to form nitrates.

Memory with Prof. Michel Che

Prof. Michel Che has been a familiar presence in the Physical Chemistry group at the Department of Chemistry in Torino. In occasion of his visits, he was available to discuss the results of younger researchers, showing sincere curiosity, interest and willingness to give suggestions and inspiration of a wider scope. He last visited Torino to receive the SCI-SCF Lectureship, from the Italian and French Chemical Societies in June 2017, giving an inspiring lecture about ‘The unifying concept of empty space in catalysis and beyond’.

Acknowledgements Tommaso Selleri (European Commission Joint Research Centre) is gratefully acknowledged for his help during the XAS experiments.

Funding Open access funding provided by Università degli Studi di Torino within the CRUI-CARE Agreement.

Open Access This article is licensed under a Creative Commons Attribution 4.0 International License, which permits use, sharing, adaptation, distribution and reproduction in any medium or format, as long as you give appropriate credit to the original author(s) and the source, provide a link to the Creative Commons licence, and indicate if changes were made. The images or other third party material in this article are included in the article's Creative Commons licence, unless indicated otherwise in a credit line to the material. If material is not included in the article's Creative Commons licence and your intended use is not permitted by statutory regulation or exceeds the permitted use, you will need to obtain permission directly from the copyright holder. To view a copy of this licence, visit <http://creativecommons.org/licenses/by/4.0/>.

References

1. J.-K. Lai, I.E. Wachs, *ACS Catal.* **8**, 7 (2018)
2. I. Nova, E. Tronconi, In: *Urea-SCR technology for deNOx after treatment of diesel exhausts*, ed. H.-Y. Chen, (Springer New York, 2014), p. 123
3. J.H. Kwak, R.G. Tonkyn, D.H. Kim, J. Szanyi, C.H.F. Peden, *J. Catal.* **275**, 2 (2010)
4. S.T. Korhonen, D.W. Fickel, R.F. Lobo, B.M. Weckhuysen, A.M. Beale, *Chem. Commun.* **47**, 2 (2011)
5. A.M. Beale, F. Gao, I. Lezcano-Gonzalez, C.H.F. Peden, J. Szanyi, *Chem. Soc. Rev.* **44**, 20 (2015)
6. E. Borfecchia, K.A. Lomachenko, F. Giordanino, H. Falsig, P. Beato, A.V. Soldatov, S. Bordiga, C. Lamberti, *Chem. Sci.* **6**, 1 (2015)
7. F. Gao, D. Mei, Y. Wang, J. Szanyi, C.H.F. Peden, *J. Am. Chem. Soc.* **139**, 4935 (2017)

8. L. Chen, T.V.W. Janssens, H. Gronbeck, *Phys. Chem. Chem. Phys.* **21**, 21 (2019)
9. H. Li, C. Paolucci, I. Khurana, L. Wilcox, F. Goltl, J.D. Albarracin-Caballero, A.J. Shih, F.H. Ribeiro, R. Gounder, W.F. Schneider, *Chem. Sci.* **10**, 8 (2019)
10. C. Paolucci, J.R. Di Iorio, W.F. Schneider, R. Gounder, *Accounts Chem. Res.* **53**, 9 (2020)
11. J.R. Di Iorio, S.C. Li, C.B. Jones, C.T. Nimlos, Y.J. Wang, E. Kunkes, V. Vattipalli, S. Prasad, A. Moini, W.F. Schneider, R. Gounder, *J. Am. Chem. Soc.* **142**, 10 (2020)
12. C. Paolucci, A.A. Verma, S.A. Bates, V.F. Kispersky, J.T. Miller, R. Gounder, W.N. Delgass, F.H. Ribeiro, W.F. Schneider, *Angew. Chem. -Int. Edit.* **53**, 44 (2014)
13. C. Paolucci, A.A. Parekh, I. Khurana, J.R. Di Iorio, H. Li, J.D. Albarracin Caballero, A.J. Shih, T. Anggara, W.N. Delgass, J.T. Miller, F.H. Ribeiro, R. Gounder, W.F. Schneider, *J. Am. Chem. Soc.* **138**, 18 (2016)
14. K.A. Lomachenko, E. Borfecchia, C. Negri, G. Berlier, C. Lamberti, P. Beato, H. Falsig, S. Bordiga, *J. Am. Chem. Soc.* **138**, 37 (2016)
15. A. Martini, E. Borfecchia, K.A. Lomachenko, I.A. Pankin, C. Negri, G. Berlier, P. Beato, H. Falsig, S. Bordiga, C. Lamberti, *Chem. Sci.* **8**, 10 (2017)
16. C.W. Andersen, E. Borfecchia, M. Bremholm, M.R.V. Jorgensen, P.N.R. Vennestrom, C. Lamberti, L.F. Lundegaard, B.B. Iversen, *Angew. Chem. -Int. Edit.* **56**, 35 (2017)
17. J.S. McEwen, T. Anggara, W.F. Schneider, V.F. Kispersky, J.T. Miller, W.N. Delgass, F.H. Ribeiro, *Catal. Today* **184**, 1 (2012)
18. T.V.W. Janssens, H. Falsig, L.F. Lundegaard, P.N.R. Vennestrøm, S.B. Rasmussen, P.G. Moses, F. Giordano, E. Borfecchia, K.A. Lomachenko, C. Lamberti, S. Bordiga, A. Godiksen, S. Mossin, P. Beato, *ACS Catal.* **5**, 2832 (2015)
19. C. Paolucci, I. Khurana, A.A. Parekh, S.C. Li, A.J. Shih, H. Li, J.R. Di Iorio, J.D. Albarracin-Caballero, A. Yezerets, J.T. Miller, W.N. Delgass, F.H. Ribeiro, W.F. Schneider, R. Gounder, *Science* **357**, 6354 (2017)
20. F. Giordano, E. Borfecchia, K.A. Lomachenko, A. Lazzarini, G. Agostini, E. Gallo, A.V. Soldatov, P. Beato, S. Bordiga, C. Lamberti, *J. Phys. Chem. Lett.* **5**, 1522 (2014)
21. L. Chen, J. Jansson, M. Skoglundh, H. Grönbeck, *J. Phys. Chem. C* **120**, 51 (2016)
22. C. Negri, T. Selli, E. Borfecchia, A. Martini, K.A. Lomachenko, T.V.W. Janssens, M. Cutini, S. Bordiga, G. Berlier, *J. Am. Chem. Soc.* **142**, 37 (2020)
23. A. Oda, H. Shionoya, Y. Hotta, T. Takewaki, K. Sawabe, A. Satsuma, *ACS Catal.* **10**, 20 (2020)
24. R. Villamaina, U. Iacobone, I. Nova, M.P. Ruggieri, J. Collier, D. Thompsett, E. Tronconi, *Chem. Cat. Chem.* **12**, 15 (2020)
25. M. Colombo, I. Nova, E. Tronconi, *Catal. Today* **197**, 1 (2012)
26. M.P. Ruggieri, I. Nova, E. Tronconi, J.A. Pihl, T.J. Toops, W.P. Partridge, *Appl. Catal. B Environ.* **166–167**, 181 (2015)
27. C. Tyrsted, E. Borfecchia, G. Berlier, K.A. Lomachenko, C. Lamberti, S. Bordiga, P.N.R. Vennestrom, T.V.W. Janssens, H. Falsig, P. Beato, A. Puig-Molina, *Catal. Sci. Technol.* **6**, 23 (2016)
28. C. Negri, P.S. Hammershøi, T.V.W. Janssens, P. Beato, G. Berlier, S. Bordiga, *Chem. Eur. J.* **24**, 46 (2018)
29. L. Chen, H. Falsig, T.V.W. Janssens, H. Gronbeck, *J. Catal.* **358**, 179 (2018)
30. A. Marberger, A.W. Petrov, P. Steiger, M. Elsener, O. Krocher, M. Nachttegaal, D. Ferri, *Nat. Catal.* **1**, 3 (2018)
31. Y. Zhang, Y. Peng, K. Li, S. Liu, J. Chen, J. Li, F. Gao, C.H.F. Peden, *ACS Catal.* **9**, 7 (2019)
32. A.G. Greenaway, A. Marberger, A. Thetford, I. Lezcano-González, M. Agote-Arán, M. Nachttegaal, D. Ferri, O. Kröcher, C.R.A. Catlow, A.M. Beale, *Chem. Sci.* **11**, 2 (2020)
33. L. Chen, T.V.W. Janssens, P.N.R. Vennestrom, J. Jansson, M. Skoglundh, H. Gronbeck, *ACS Catal.* **10**, 10 (2020)
34. M.P. Ruggieri, J. Luo, I. Nova, E. Tronconi, K. Kamasamudram, A. Yezerets, *Catal. Today* **307**, 48 (2018)
35. J. Szanyi, J.H. Kwak, H. Zhu, C.H.F. Peden, *Phys. Chem. Chem. Phys.* **15**, 7 (2013)
36. C. Negri, E. Borfecchia, M. Cutini, K.A. Lomachenko, T.V.W. Janssens, G. Berlier, S. Bordiga, *Chem. Cat. Chem.* **11**, 16 (2019)
37. M.P. Ruggieri, T. Selli, I. Nova, E. Tronconi, J.A. Pihl, T.J. Toops, W.P. Partridge, *Top. Catal.* **59**, 10 (2016)
38. P.S. Hammershøi, C. Negri, G. Berlier, S. Bordiga, P. Beato, T.V.W. Janssens, *Catal. Sci. Technol.* **9**, 10 (2019)
39. A. Martini, E. Borfecchia, *Crystals* **10**, 8 (2020)

40. O. Mathon, A. Beteva, J. Borrel, D. Bugnazet, S. Gatla, R. Hino, I. Kantor, T. Mairs, M. Munoz, S. Pasternak, F. Perrin, S. Pascarelli, J. Synchrotron Rad. **22**, 6 (2015)
41. D. Bellet, B. Gorges, A. Dallery, P. Bernard, E. Pereiro, J. Baruchel, J. Appl. Crystallogr. **36**, 366 (2003)
42. C. Lamberti, S. Bordiga, F. Bonino, C. Prestipino, G. Berlier, L. Capello, F. D'Acapito, F. Xamena, A. Zecchina, Phys. Chem. Chem. Phys. **5**, 20 (2003)
43. S. Bordiga, E. Groppo, G. Agostini, J.A. van Bokhoven, C. Lamberti, Chem. Rev. **113**, 3 (2013)
44. B. Ravel, M. Newville, J. Synchrotron Rad. **12**, 4 (2005)
45. J. Jaumot, R. Gargallo, A. de Juan, R. Tauler, Chemometrics Intell. Lab. Syst. **76**, 1 (2005)
46. C. Ruckebusch, *Resolving Spectral Mixtures: With Applications from Ultrafast Time-Resolved Spectroscopy to Super-Resolution Imaging* (Elsevier, Amsterdam, 2016).
47. M. Fernandez-Garcia, G.L. Haller, J. Phys. IV **7**, C2 (1997)
48. W. Windig, J. Guilment, Anal. Chem. **63**, 14 (1991)
49. P. Conti, S. Zamponi, M. Giorgetti, M. Berrettoni, W.H. Smyrl, Anal. Chem. **82**, 9 (2010)
50. J.P. Perdew, K. Burke, M. Ernzerhof, Phys. Rev. Lett. **77**, 18 (1996)
51. ADF, *SCM Theoretical Chemistry* (Vrije Universiteit, Amsterdam, 2012).
52. G. te Velde, F.M. Bickelhaupt, E.J. Baerends, C.F. Guerra, S.J.A. Van Gisbergen, J.G. Snijders, T. Ziegler, J. Comput. Chem. **22**, 9 (2001)
53. G. Smolentsev, A.V. Soldatov, J. Messinger, K. Merz, T. Weyhermuller, U. Bergmann, Y. Pushkar, J. Yano, V.K. Yachandra, P. Glatzel, J. Am. Chem. Soc. **131**, 36 (2009)
54. I. Alperovich, G. Smolentsev, D. Moonshiram, J.W. Jurss, J.J. Concepcion, T.J. Meyer, A. Soldatov, Y. Pushkar, J. Am. Chem. Soc. **133**, 39 (2011)
55. K.A. Lomachenko, C. Garino, E. Gallo, D. Gianolio, R. Gobetto, P. Glatzel, N. Smolentsev, G. Smolentsev, A.V. Soldatov, C. Lamberti, L. Salassa, Phys. Chem. Chem. Phys. **15**, 38 (2013)
56. E. Borfecchia, P. Beato, S. Svelle, U. Olsbye, C. Lamberti, S. Bordiga, Chem. Soc. Rev. **47**, 22 (2018)
57. L.S. Kau, D.J. Spirasolomon, J.E. Pennerhahn, K.O. Hodgson, E.I. Solomon, J. Am. Chem. Soc. **109**, 21 (1987)
58. M. Sano, S. Komorita, H. Yamatera, Inorg. Chem. **31**, 3 (1992)
59. E.I. Solomon, D.E. Heppner, E.M. Johnston, J.W. Ginsbach, J. Cirera, M. Qayyum, M.T. Kieber-Emmons, C.H. Kjaergaard, R.G. Hadt, L. Tian, Chem. Rev. **114**, 7 (2014)
60. E. Borfecchia, C. Negri, K.A. Lomachenko, C. Lamberti, T.V.W. Janssens, G. Berlier, React. Chem. Eng. **4**, 6 (2019)
61. G. Lambie, A. Moen, D.G. Nicholson, J. Chem. Soc. Faraday Trans. **90**, 15 (1994)
62. L. Chen, T.V.W. Janssens, M. Skoglundh, H. Grönbeck, Top. Catal. **62**, 1 (2019)

Publisher's Note Springer Nature remains neutral with regard to jurisdictional claims in published maps and institutional affiliations.



Chiara Negri



Elisa Borfecchia



Andrea Martini



zGabriele Deplanov



Kirill A. Lomachenko



Ton V. W. Janssens



Gloria Berlier



Silvia Bordiga

Affiliations

Chiara Negri^{1,5} · Elisa Borfecchia¹ · Andrea Martini^{1,2} · Gabriele Deplano¹ · Kirill A. Lomachenko³ · Ton V. W. Janssens⁴ · Gloria Berlier¹ · Silvia Bordiga¹

✉ Gloria Berlier
gloria.berlier@unito.it

¹ Department of Chemistry and NIS Centre, University of Turin, Via Giuria 7, 10125 Turin, Italy

² Smart Materials, Research Institute, Southern Federal University, Sladkova Street 174/28, Rostov-on-Don, Russia 344090

³ European Synchrotron Radiation Facility, 71 Avenue des Martyrs, CS 40220, 38043 Grenoble Cedex 9, France

⁴ Umicore Denmark ApS, Kogle Allé 1, 2970 Hørsholm, Denmark

⁵ Present Address: Department of Chemistry, Center for Materials Science and Nanotechnology, University of Oslo, Sem Sælands vei 26, 0371 Oslo, Norway